Exploration of Li-Ion Batteries during a Long-Term Heat Endurance Test Using 3D Temporal Microcomputed Tomography Investigation

Gergő Ballai, Milán Attila Sőrés, Lívia Vásárhelyi, Imre Szenti, Robert Kun, Bálint Hartmann, Dániel Sebők, Ferenc Farkas, Aqib Zahoor, Guozhu Mao, András Sápi,* Ákos Kukovecz, and Zoltán Kónya

High-resolution computed tomography (micro-CT) was used in this paper to visualize the inner structure of lithium nickel cobalt aluminum oxide 18 650 form-factor batteries non-destructively after and during a heat endurance test. Open circuit relaxation and electrochemical impedance spectroscopy were also conducted. We tested the different heat-aged cells with micro-CT and charge-discharge and electrochemical impedance spectroscopy measurements to find the observable physical changes in the cell and connect them to the loss of performance. We found that the drastic changes in the structure of the cell at higher temperatures are well traceable. At 150 °C layer delamination and performance loss were observed, battery failure occurred with the further increase of the temperature, while at the same time, precipitation appeared and the positive temperature coefficient device fractured. Without opening the cell only tomographic methods can provide insight into the inner structure of the cell. We were able to measure the changes in the distances of the layers of the battery and decent shrinkage was observed, which can be linked to the loss of capacity and increased resistance.

1. Introduction

Lithium-ion batteries (Li-ion batteries, LIBs), due to their high power and energy densities, are very important energy storage devices used for many mobile and also for stationary applications. They are routinely used in commercially available portable devices (e.g., smartphones, laptops, e-cigarettes), thus ensuring their safe operation is a top priority, especially since they contain highly reactive, flammable, and sensitive materials, such as the organic Li-ion electrolyte. Several factors can cause the failure of Li-ion batteries, some of which only result in malfunction (i.e., non-energetic failure modes), while others can lead to the dangerous thermal runaway and the explosion of the batteries (i.e., energetic failure modes). Li-ion battery cells can be exposed to mechanical, electrical and thermal abuse, in general. Short-circuited,

G. Ballai, L. Vásárhelyi, I. Szenti, D. Sebők, A. Sápi, Á. Kukovecz, Z. Kónya
Interdisciplinary Excellence Centre
Department of Applied and Environmental Chemistry
University of Szeged
H-6720 Szeged, Hungary
E-mail: sapia@chem.u.szeged.hu

M. A. Sőrés, B. Hartmann
Centre for Energy Research
Institute for Energy Security and Environmental Safety
H-1121 Budapest, Hungary

I. Szenti, Z. Kónya
Hungarian Academy of Sciences
MTA-SZTE Reaction Kinetics and Surface Chemistry Research Group
H-6720 Szeged, Hungary

The ORCID identification number(s) for the author(s) of this article can be found under https://doi.org/10.1002/ente.202300207.

R. Kun
Institute of Materials and Environmental Chemistry
Research Centre for Natural Sciences
H-1117 Budapest, Hungary

R. Kun
Department of Chemical and Environmental Process Engineering
Faculty of Chemical Technology and Biotechnology
Budapest University of Technology and Economics
H-1111 Budapest, Hungary

F. Farkas
Faculty of Engineering
University of Szeged
H-6720 Szeged, Hungary

A. Zahoor, G. Mao
School of Environmental Science and Engineering
Tianjin University
Tianjin 300350, China

A. Zahoor, G. Mao
National Industry-Education Platform of Energy Storage
Tianjin University
Tianjin 300072, China

overcharged, or over-discharged batteries (electrical abuse), for example, can enter a dangerous self-inducing exothermic reaction cascade, known as thermal runaway. Other abuse conditions, such as mechanical deformation, or foreign body penetration (mechanical abuse) can also cause cell internal shorting, thereby may result in heat evolvement and eventually may cause thermal runaway.[1] The thermal runaway process can lead to a battery temperature rise of 600 °C in extreme cases. It was found that the thermal runaway can be triggered by increasing the ambient temperature (thermal abuse). Raising temperature, already above ≈70–80 °C causes the solid electrolyte interface (SEI) to decompose. The simultaneous electrolyte decomposition results in heat release and formation of gaseous by-products within the battery cell. Further heating of the battery cell beyond this temperature results in more severe safety conditions and thermal runaway will occur. There is an onset temperature, on which thermal runaway will certainly occur, which is between 145 and 150 °C for cylindrical 18 650 cells,[2] based on the results of thermal abuse tests.

To improve the safety and performance of LIBs a thorough understanding of their internal 3D structure, mainly the electrode stack's (folded or rolled) microstructural condition is indispensable. The real and in-operando 3D internal structure of the samples can be visualized by high-resolution computed tomography (micro-CT), neutron tomography or 3D X-ray microscopy.[3–5] Micro-CT is an important non-destructive, 3D X-ray visualization technique in materials science,[6] based on the differing X-ray attenuation of materials. It is especially suitable for the visualization of Li-ion batteries internal (micro-)structure while sustaining the real physical conditions of the analyzed cells. Micro-CT renders the investigation of real 3D structure possible, and its non-destructive nature also allows us to conduct temporal investigations. The possibility of temporal investigations (also referred to as 4D micro-CT) gives opportunities to investigate the effect of external/internal impacts on the structure of batteries, e.g., compression,[7] nail intrusion,[8] heat treatment,[9] overcharge[10] or thermal runaway.[10] If the changes are applied outside the micro-CT device it is called ex-situ measurement, while by using special cells, in-situ measurements can also be conducted, which can be either interrupted or continuous[11]; thereby energy storage devices can even be investigated in-operando conditions. In-operando measurements require extremely short image acquisition times, thus high flux/intensity is needed, which can be achieved in synchrotron facilities.[12] Regular laboratory-based CTs with an X-ray tube, however, can also provide valuable information regarding the detailed structure of the batteries, with micron-scale resolution. The quality of these longer measurements also tends to be better than that of the quasi-real-time images, thus preferable for investigating processes with a longer time span.

Micro-CT is routinely used as a characterization tool in the fields of energy storage and conversion.[4,11–13] Micro-CT can help to identify the effect of microstructural[14,15] inhomogeneity on the performance of Li-ion batteries.[5,16] The thermal runaway process of LIBs can be investigated in real-time within operando micro-CT.[9] Post-mortem micro-CT investigation can also provide valuable information: the examination of exploded batteries, for example, can give an insight into the processes/structural changes that caused the explosion.[17] Other than lithium-ion batteries lithium iron phosphate batteries[18] and lithium-sulfur batteries[19] can also be investigated.

Experiences of such examinations can be directly utilized in many fields, including the prolonging of battery lifetime of Li-ion batteries used in stationary battery energy storage systems. The global demand for such units is estimated to reach 2623 GWh by 2030 according to European Commission,[20,21] and understanding the factors behind degradation can not only contribute to the sizing of those, but also to the optimization of electricity market services provided by batteries.[22]

In this article, commercial, Panasonic NCR18650BD form factor Li-ion battery cells are investigated under thermal abuse conditions and its temperature- and time-dependent microstructural changes are investigated using micro-CT analysis, supplemented by charge-discharge and electrochemical impedance spectroscopy measurements, at some selected heat abuse temperatures, to quantify its effects. The batteries are exposed to gradual heat treatment and their open-circuit voltage (OCV) is monitored over time. The threshold temperature is determined where the battery performance started to decrease. The structural changes induced by the high temperature are characterized by multiple micro-CT measurements and a possible explanation is given to the failure of investigated Li-ion batteries at elevated temperatures. We were the first who found correlation between the decrease in the layer distances of the cell and the decaying performance following high temperatures.

2. Experimental Section

The long-term external heat treatment experiments were performed on cylindrical Panasonic NCR18650BD Li-ion batteries with a nominal capacity of 3030 mAh at the state of health (SOH) of 100%, as follows: the new batteries, in factory condition (SOC, state of charge at ≈60%), were heated in a thermostatically controlled oven (VWR DRY-Line 180 Prime) from 75 to 165 °C, increased in steps of 15 °C every 8 days. Micro-CT and voltage measurements (Keithley 2401 source meter) were conducted every 2 days to examine the structural and performance changes caused by the heat treatment. In all the cases the cells were cooled down to room temperature before measurements.

Ex-situ temporal micro-CT measurements were conducted with a Bruker Skyscan 2211 using 155 kV and 70 μA for X-ray generation, including 0.5 mm Ti beam filters, at a resolution of 11 μm³/voxel. To be able to achieve this high resolution, over-size scan mode had to be applied, we automatically divided the sample into 6 equal parts and reconnected them during reconstruction by the software. X-ray projection images were recorded at 50 ms per image, with 1113 images per section in 0.2° stepwise rotation of the sample. NRecon reconstruction software (Skyscan, Bruker, Belgium) was used to reconstruct the projected images and CTVox (Skyscan, Bruker, Belgium) and DataViewer (Skyscan, Bruker, Belgium) software were used for the visualization of the 3D-rendered objects.

The electrical performance and capabilities of a fresh (BOL, beginning-of-life) cell and a cell treated at 120 °C were compared. This temperature was chosen because according to Figure 3. beyond 135 °C OCV measurements indicate severe deterioration of the cell's internal structure. According to[23] 120 °C is the

ADVANCED
SCIENCE NEWS
www.advancedsciencenews.com

Energy Technology
Generation, Conversion, Storage, Distribution

www.entechnol.de

upper limit where the SEI layer can block the contact between anode and electrolyte, however, it is well beyond the optimal working limit, as SEI has already started to decompose. At this temperature, the heat damage is already significant, but the cell remains operational with a significantly decreased performance. Standardized tests, such as electrochemical impedance spectroscopy (EIS), can still be performed. In our study, three types of measurements were determined to characterize the heat treatment effects on the cell. Capacity measurement, OCV relaxation and EIS. Each test was performed on both new cells and heat-treated cells, by a Metrohm Autolab PGSTAT302n potentiostat at room temperature, which was $22\,°C \pm 2\,°C$ in our study. The batteries were enclosed in a custom-made 3D printed battery holder tightened by brass screws for proper contact.

2.1. Capacity Measurements

The capacity measurements consisted of three stages. At the first stage, there was the initial charge of the cells from the capacity after shipment to 100% SOC. It was done by standard CC-CV charging method with 0.3C (909 mA) constant current, and 4.2 V constant voltage, with 0.02C or C/50 (60 mA) cut-off current. After 24 h rest period, a CC discharge phase is followed with 0.1C or C/10 (303 mA) and a cut-off voltage of 2.5 V. The last step was CC-CV charging with 0.1 C or C/10 (303 mA), and a 4.2 constant voltage phase, the same as in the case of the initial charge. **Table 1** summarizes the methods and applied limits, as well as the derived quantities.

From this measurement discharge and charge capacities were determined by the Coulomb counting method Equation (1).

$$Q = \int_{\tau_0}^{\tau_1} i(t)\mathrm{d}t \tag{1}$$

where Q is the capacity, $i(t)$ is current, τ_0 is the start of the charge-discharge measurement and the end of the measurement is τ_1, which is the time when the battery reaches the end conditions. For discharge, that means the cut-off voltage limit is 2.5 V. For charge it means the 0.02C (50 mA) charging current. The direction of the current is not considered in this formula, discharge and charge capacity are denoted by Q_{dsch} and Q_{chg} respectively. We assume that after the initial charge stage, the cell is at SOC = 100%, while after discharge the SOC = 0%.

Table 1. The procedure of the capacity measurements.

Step No.	Stage	Method	End condition	Derived Quantity
1.	Initial Charge	CC	4.2 V	–
2.	Initial Charge	CV	0.02C or C/50 (60 mA)	
3.	Relax for 24 h	–		–
4.	Discharge	CC	2.5 V (low cut-off)	Discharge capacity
5.	Charge	CC	4.2 V (high cut-off)	Charge capacity
6.	Charge	CV	0.02C or C/50 (60 mA)	Charge capacity

2.2. OCV Relaxation

Voltage relaxation (OCV retention) in open circuit conditions was monitored for 24 h during the relaxation period between the initial charge phase and the CC discharge. The SOC of the battery cells for this measurement is considered to be 100%. OCVs were recorded each hour, providing information on the current state-of-health of the cell and indicating the expected self-discharge as well. Although storing cells at that high SOC are considered to accelerate capacity fade, for such a short period, this can be neglected.

2.3. EIS Measurements

Electrochemical impedance spectroscopy measurements were done completely separately from the discharge measurements. Two different EIS were performed. The first one was at 100% SOC for 25, 60 and 120 °C. and the second, at 120 °C at three different SOC levels: 0%, 50% and 100%, from 4 kHz to 0.01 Hz. The steps for the frequency sweep were 10 points per decade. The impedance of the battery is calculated by Equation (2).

$$\overline{Z} = \frac{\overline{V}}{\overline{I}} = \frac{|V|\exp(j\omega t + \varphi_V)}{|I|\exp(j\omega t + \varphi_I)} = |Z|\exp(\varphi_Z) = Z' + jZ'' \tag{2}$$

This is the general definition of the impedance, in the case of an AC system. Impedance ($\overline{Z}$) is the quotient of the complex voltage ($\overline{V}$) and current ($\overline{I}$). We can write the complex numbers in polar coordinate form, with an absolute value and a phase angle (φ). Here the absolute value of the complex impedance will be the quotient of the absolute value of voltage and current, while the phase shift will be the difference between the voltage phase and current phase. This can be rewritten as a Cartesian form, the real value can be implemented as the resistance (Z'), while the complex value as the reactance (Z''). Specifically for batteries, the reactance is capacitive in the lower frequency ranges. Note that in electrical engineering publications, j is used instead of i, for the complex unit, as i is reserved for current.

To measure the change in the electrochemical properties of cells three cells were measured. One after 120 °C, one after 60 °C and one after 25 °C for one week. The three temperatures were chosen to represent the unbothered cell, the temperature abuse resulting from average use and extreme heat abuse. The electrochemical measurements as the charge-discharge measurements and the electrochemical impedance measurements were conducted by using a Merohm Autolab PGSTAT302N potentiostat.

The charge-discharge measurements were recorded at 0.1C-rate to evaluate the heat damage that can cause the decrease in the capacity. The upper and lower cut of voltages were 4.2 and 2.5 Volts, respectively.

The EIS measurements were recorded by the same setup between 2500 and 0.1 Hz with the applied signal amplitude of 0.01 of the V_{RMS}.

Post-mortem energy dispersive spectroscopy (EDS) measurement was used to determine the elemental composition of the layers. The sample preparation required an inert atmosphere, thus the preparation was conducted in an Ar (Messer 5.0) filled glove box. An intact battery was embedded in resin and cut into

1 cm high pieces. The elemental composition of the battery parts was analyzed by energy-dispersive X-ray spectroscopy (Röntec Quantax EDS) built into a Hitachi S-4700. The samples were measured at 20 kV accelerating voltage without any additional coating.

3. Results and Discussion

3.1. Structural Analysis

A 3D structural analysis of the 18 650 Li-ion batteries was conducted by micro-CT. The typical layered structure of cylindrical LIBs is shown in **Figure 1**. On the top, the parts of the cathode are visible: the top cover, the gasket seal, the current interrupt device (CID) (parts of which are the top disk, the insulator, the bottom disk, and the tab), and the positive temperature coefficient (PTC) device. On the bottom side, the anode pole can be seen (the anode tab and the bottom insulator). The two poles are connected by the center pin and a coiled structure (also called a jelly roll structure), which can be seen on the enlarged part on the right. This contains the anode, the cathode, and the separator layers. The whole structure is enclosed into a steel can.

Figure 2 shows a horizontal cross section of a 3D micro-CT image of the Li-ion battery. The typical circular jelly roll structure of the Li-ion batteries can be seen on the left, while the enlarged part also shows the EDS element mapping results. Micro-CT alone is not capable of element analysis, but by combining it with EDS we can gain insight into the 3D element composition of Li-ion batteries. This representation enables the identification
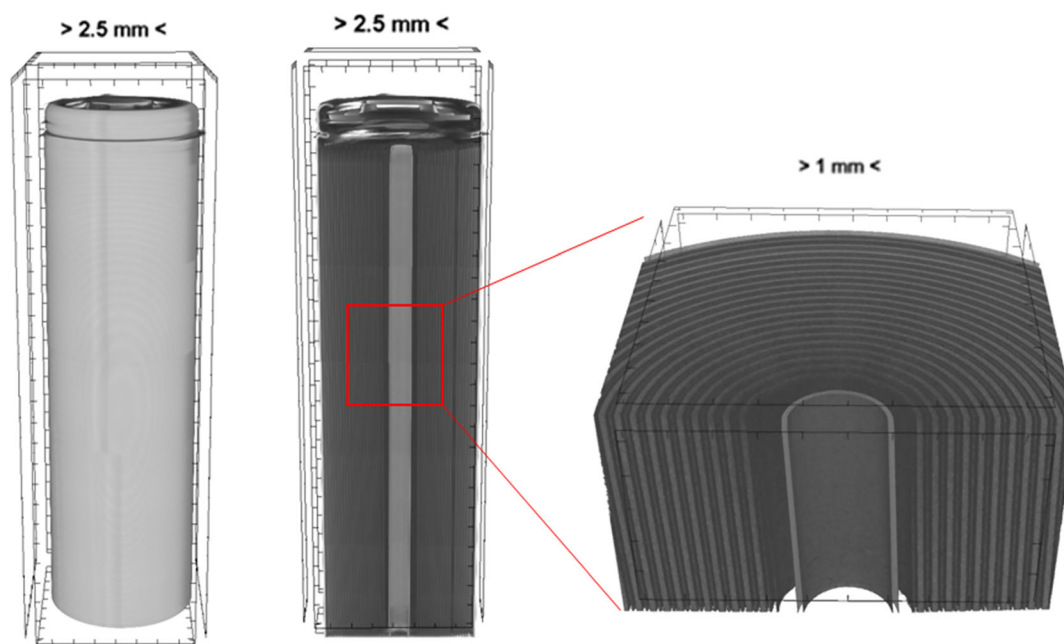

Figure 1. 3D Micro-CT reconstructed images of a 18 650 Li-ion battery, taken with 11 µm³/voxel resolution: an outside view of the steel can, a vertical cross section of the inner structure, and an enlarged view of the jelly roll structure.
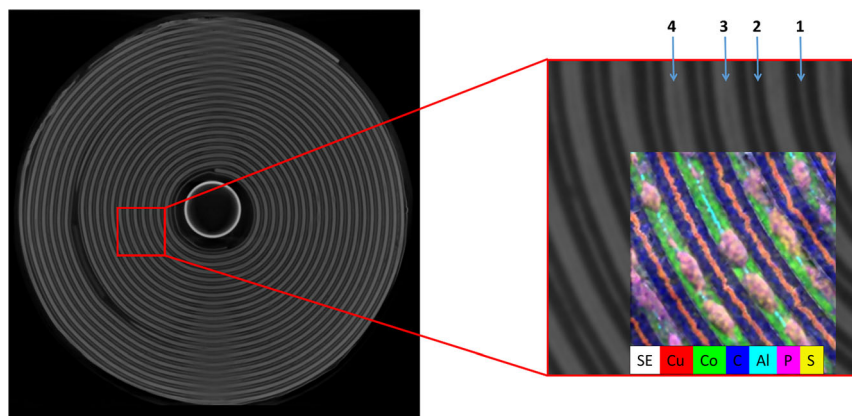

Figure 2. A horizontal cross section of a 3D micro-CT image of a 18 650 Li-ion battery, taken with 11 µm³/voxel resolution. The enlarged part also shows the EDS element mapping results on top of the micro-CT image.

ADVANCED
SCIENCE NEWS
www.advancedsciencenews.com

Energy Technology
Generation, Conversion, Storage, Distribution
www.entechnol.de

of the element composition of the layered structure visible on the micro-CT image. The copper foil (1), carbon in the anode's layer (2), cobalt originating from the cathode (3), and aluminum foil (4) layers are well separated and identified.

Figure 3 shows the measured cell voltages at ≈50% SOC, at different temperatures (after 8-day heat treatment). The measured voltages of around 3.5 V are the expected values according to the specification of the rechargeable 18 650 Li-ion batteries. The OCV of the battery is unaltered up to 135 °C, but at 150 °C, a rapid decrease in the OCV was observed. The voltage was already

decreased at the first measurement (after 2 days) and did not alter during the 8-day cycle. In contrast to the previous stages, at 165 °C, a visible change occurred in the condition of the battery: cell opening occurred and this resulted in electrolyte leakage. After that, no OCV was measurable, and the cell was irreversibly destroyed before a thermal runaway reaction occurred.

Figure 4 shows the structural deformations caused by external overheating. There was no visible change in the structure at 135 °C compared to room temperature. The first changes occurred at 150 °C, after 2 days of heating; further deformation did not occur until the end of the 8-day heating cycle. The overheating can also cause delamination and layer deformation (of the Cu layer); these are visible on the figure (blue box) and can cause short-circuiting and thus battery failure. Increasing the temperature to 165 °C showed that layer deformation was not observed, but additional
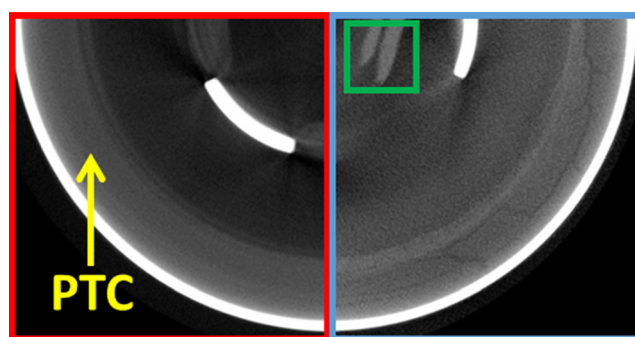

Figure 3. The measured OCVs of the cells versus the temperature of the long-term heat treatment experiments.

Figure 5. Condition of the PTC after 150 (red box) and 165 °C (blue box) external heat treatment; green box highlights the formed precipitation due to leakage. The micro-CT images were taken with 11 µm^3/voxel resolution.
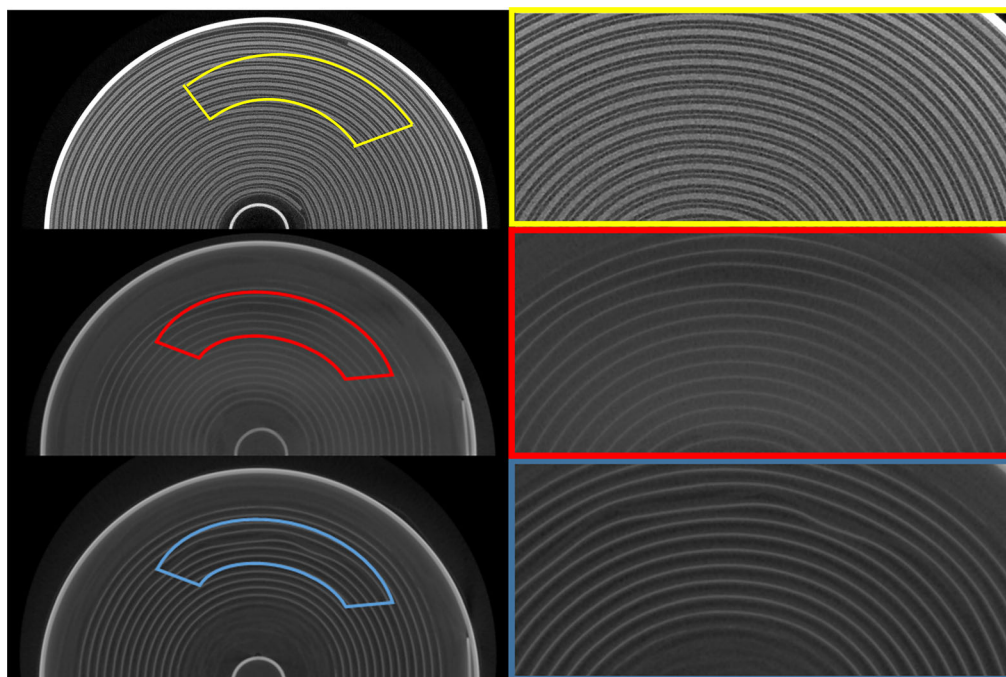

Figure 4. Micro-CT images of structural changes in the layers of 18 650 Li-ion battery caused by external overheating taken with 11 µm^3/voxel resolution compared to the unaltered cell. The upper part shows the structure of the unaltered cell (yellow box), the middle one at 135 °C (red box), and the lower one at 150 °C (blue box).

**ADVANCED
SCIENCE NEWS**

www.advancedsciencenews.com

Energy Technology
Generation, Conversion, Storage, Distribution

www.entechnol.de

deformations did occur. In **Figure 5**, the PTC device of the battery is shown at 150 and 165 °C. At the lower temperature, the PTC appears to be intact, while at higher temperature, the PTC is heavily fractured. At 165 °C, while no traces of external damage were observed, a leakage through the pressure seal occurred, exposing the electrolyte to oxygen, causing precipitation formation as seen on the upper part framed by a green box.

Multiple research has addressed and examined the structural changes during and after a thermal runaway reaction of commercial batteries with the micro-CT technique.[17,24] We found that noticeable changes occur even without the dangerous energetic reactions.

Blazek et al. reported the swelling of the electrode stack as a result of prolonged use which can further accelerate the aging of the battery cells. They found that this phenomenon can be tracked by micro-CT measurements by measuring the distance between the layers in a cross-sectional view of the cell without opening it. Significant increases in the distances were found in the used cells with similar SOCs.[25] To learn if similar phenomena take place in batteries during extreme heat exposures, the layer distances of the cells after different temperature exposures were measured (**Figure 6**).

By measuring and averaging the thickness of ten layers in eight directions radially from the middle of the cell, we found that the average distance decreases by 1.61% from the initial value of $354.0 \pm 1.3\,\mu m$ to $348.3 \pm 1.5\,\mu m$. Blazek et al. experienced a similar change in magnitude, although in the other direction.[25] This can be linked to the different processes involved during their measurements in the repeatedly charged and discharged and our heat-stressed cells. The decreases that we have experienced in the layer thickness can be linked to the degradation of the porous anode and cathode materials, by the exposure to the increased temperature and the consequential increased pressure inside the cell.

3.2. Capacity Measurements Results

Capacity measurements were performed at four chosen temperatures: 25, 60, 120, and 150 °C summarized in **Table 2**.

Although both discharge and the charge capacity are slightly higher in the case of the 60 °C heat-treated cell, these values are within the rated capacity (20 °C) and the typical capacity (25 °C) of the NCR18650BD cell, set by the manufacturer. These

Table 2. The charge and discharge capacity of the cells after 1 week of heat abuse at different temperatures.

Temperature [°C]	Capacity discharge [Ah]	Capacity charge [Ah]
25	2.973	2.913
60	3.171	3.108
120	2.713	2.738
150	n.a.	n.a.

variations occur due to small differences in cells or the room temperature because available capacity for a given constant current discharge rate is temperature dependent, and it is typical for higher temperatures to result in more capacity.[26] However, after a heat abuse at 120 °C, capacity decay is observable and significant, around 10% to the nominal value. At 150 °C, no detectable cell capacity was observed due to the aforementioned irreversible destruction of the battery.

3.3. OCV Relaxation Measurement Results

The OCV relaxation measurements were designed originally for 4 different temperatures 25, 60, 120, and 150 °C. But as shown in Figure 3. at 150 °C the OCV is quite unstable, indicating that such physical changes occurred inside the cell, that no charge–discharge measurements can be performed on it, and therefore neither OCV relaxation tests. Consequently, only the first three measurements will be presented in **Figure 7**.

For the initial OCV, there is no significant difference between the different temperatures. As the temperature is increased, the relaxation occurs faster and at 120 °C, it turns to a more elevated self-discharge scenario.

3.4. EIS Measurement Results

As previously mentioned, two types of EIS measurements were conducted. These will be discussed separately.

3.4.1. EIS at SOC 100%

In the first measurement, the EIS was conducted at different temperatures, with a fully charged cell, which is shown in
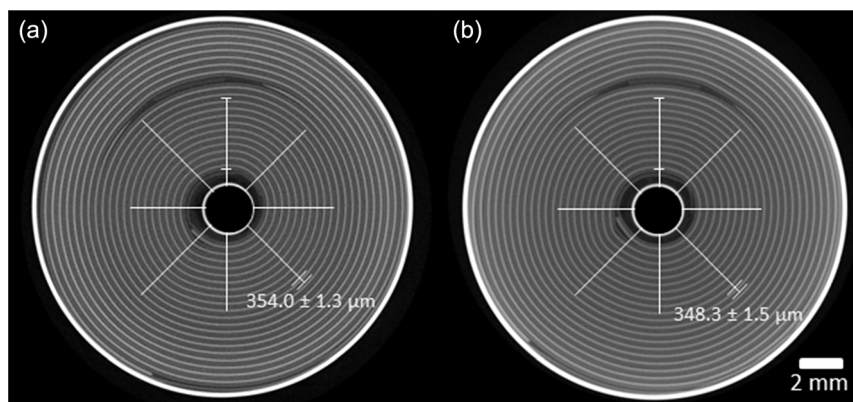

Figure 6. a) The cross-sectional view of the unaltered and b) the 150 °C heat-treated cell.
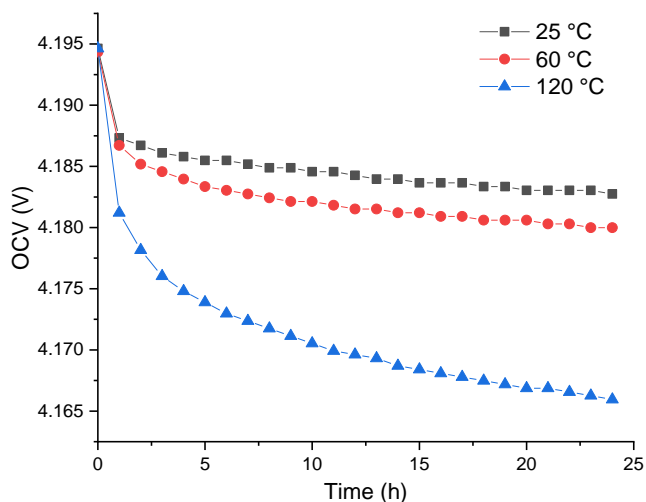
Figure 7. The measured OCVs of the fully charged cells in a period of 24 h.

high-frequency range, we can observe the impedance (mostly inductive) of the electrical connection, and when $Z'' = 0$ the ohmic resistance of the cell. In the middle range, semicircles connected to SEI, charge transfer, and electrochemical double layer can be observed. Usually, the semicircle at higher frequencies is described as the impedance of the SEI layer and the other at lower frequencies is linked to the charge-transfer reaction. Although the regions representing SEI layer and double layer are "merged" into one semicircle in the case of the cell exposed at 120 °C, as opposed to the theoretical EIS curve,[28] this is not a unique measurement result. Li et al. claimed that it happens when no charge transfer reactions occur at the interfaces.[29] This phenomenon is well described in the literature.[30–32] Then at the lower-frequency domain, mass transport that is usually represented with the so-called Warburg impedance is also observable.[33]

As the difference between 25 and 60 °C, a little ohmic resistance increase can be observed at the higher range of the frequency. The difference for lower frequencies is negligible. However, for 120 °C, middle-frequency phenomena overlap into one semicircle. Another notable effect is that the ohmic resistance of the cell has grown to almost 150% compared to the unaltered cell (from 42.3 to 61.1 milliohms). The ohmic resistance or bulk resistance of the cell is generally considered one of the indicators to determine the state of health of cells as it tends to increase due to crack formation in the electrodes and the attrition
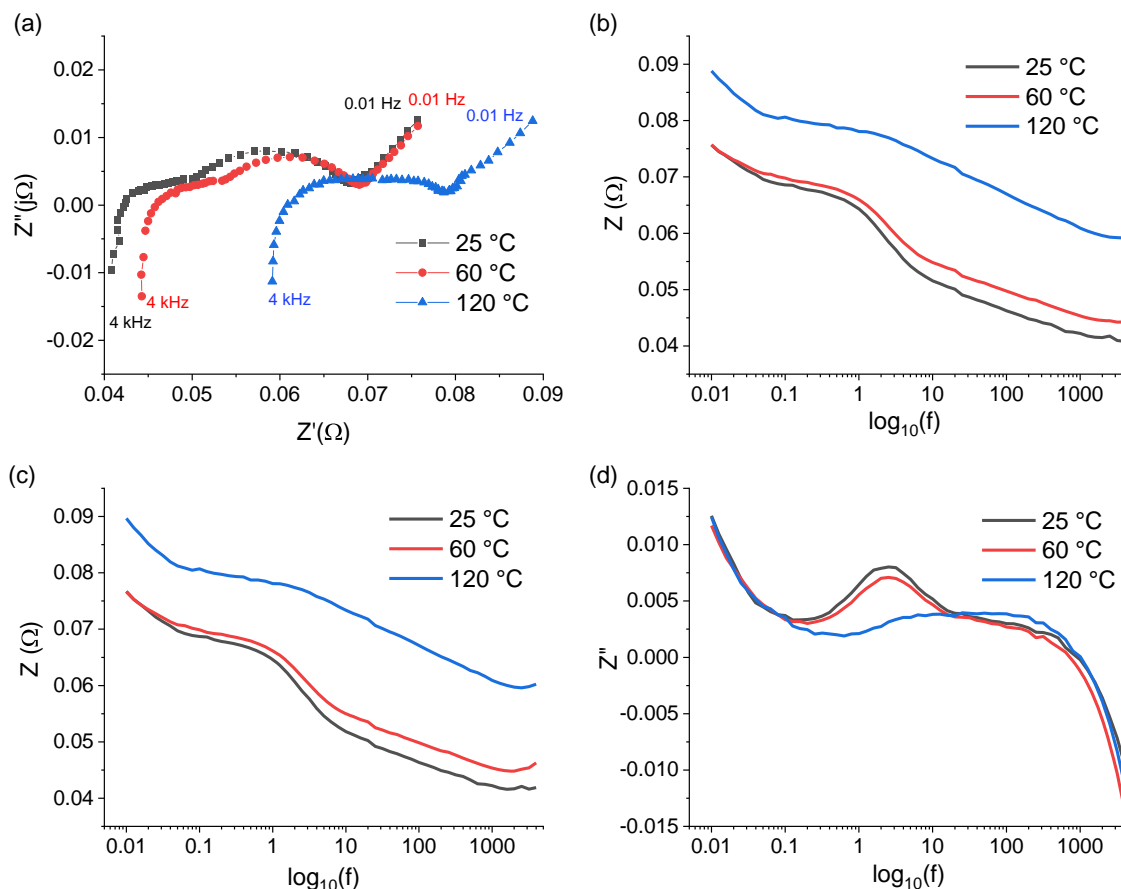
Figure 8a. The results for 25 and 60 °C show a Nyquist plot of a Li-ion battery cell. For all the temperatures, the usual frequency domains, high- ($f > 1\,\text{kHz}$), middle ($1\,\text{kHz} > f > 1\,\text{Hz}$)- and, low-frequency domains ($f < 1\,\text{Hz}$), are distinguished.[27] At the

Figure 8. a) EIS at different temperatures with fully charged cells, b) the real part of the cell impedance at different frequencies, c) the magnitude of the cell impedance at different frequencies, and d) the imaginary part of the impedance at different frequencies.

of the electrolyte.[34] At the same time, the polarization resistance decreased with the increasing heat treatment temperatures. The experienced growth in internal resistance and loss of capacity after higher temperatures can be linked to several factors, for example, increasing electrolyte viscosity, decomposition of the SEI layer,[35] degradation of the electrode materials, or the decrease in the quantity of lithium that can be used in the reaction. The battery becomes short circuited between 120 and 140 °C because of the melting of the polymer separator and the degradation of the PTC.[36]

For the real and imaginary parts of the impedance, there is a difference in order, and the real part of the impedance is much greater. That is why we got almost the same plots when observing the magnitude of Z ($|Z|$) and Z', as shown in Figure 7b,c. Different electrochemical phenomena affect the imaginary part of the impedance (Z'') much, as shown in Figure 8d.

3.4.2. EIS at 120 °C

In the second measurement, the EIS is conducted at different SOCs, with a cell at 120 °C, at the beginning of life, which is shown in **Figure 9**.

In this case, a significant increase in the real part of impedance can be observed between 100% SOC and 50% SOC. However for 0% SOC, there is no further increase in the ohmic resistance, but with lowering frequencies the impedance tends to infinity, with $Z' = 0.211$ [Ω] and $Z'' = 0.575$ [Ω] at 0.01 Hz. This increase at a very low charge of the cell is also expected based on the literature.[37]

For the relation between the magnitude of Z and Z' the same can be stated as in the previous case, which is shown in Figure 9. In figure of Z'' the effects of different electrochemical processes are completely blurred, because of the rapid increase. The experienced increase in internal resistance and loss of capacity can be linked to several factors. These physical changes possibly can be linked to the change in layer thickness which can be observed by computer tomographic measurements.

4. Conclusion

The effect of long-term elevated external temperature on the 3D structure of 18 650 Li-ion batteries was examined by ex situ temporal micro-CT investigation. Micro-CT proved to be a capable tool to investigate the internal structure of LIBs and detect the signs of degradation in the PTC of the cell which can be a sign of exposure to extreme temperatures or prolonged use. It showed in cell diagnostics it can be used for prevention and not just operando or postaccident investigation. External overheating caused serious damage to the electrode layer structure of the batteries. The temperature-induced structural deformation of the layers
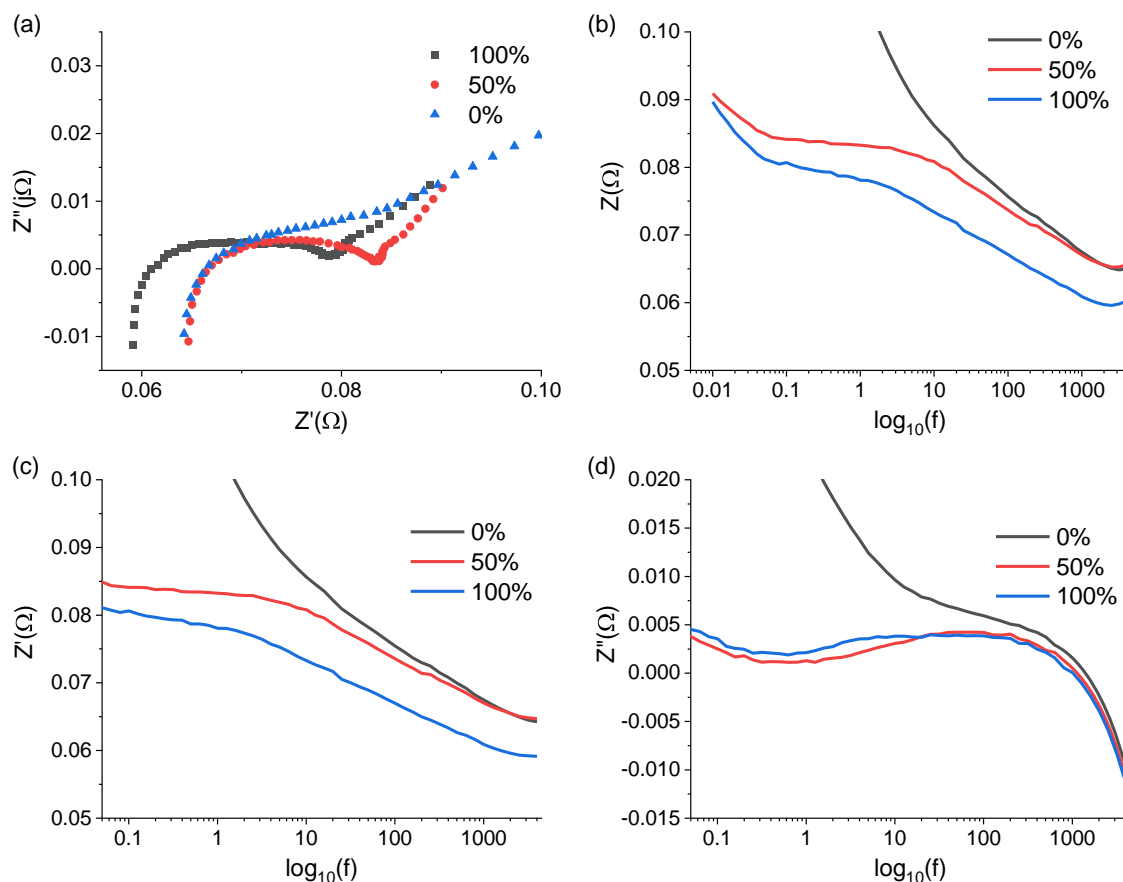

Figure 9. EIS at different SOCs at 120 °C (a), the magnitude (b), the real part (c), and the imaginary part (d) of the cell impedance at different SOCs.

started at 150 °C causing short circuiting and malfunction. However, the charge–discharge and EIS measurements show that the capacity loss and the increase of the battery resistance start at a much lower temperature; at the same time decrease in the distance between the layers in the rolled-up cell was observed on the micro-CT images. Further heat treatment caused leakage, the fracturing of the PTC layer, and the total failure of the battery. It was demonstrated that by micro-CT even slight changes in the structure can be perceived even before the dangerous thermal runaway, which could not be investigated by computed tomography or related techniques, and it has its place among other approaches to evaluating used battery cells and to find changes in the micrometer range. Smaller changes only can be observed by opening the cell. Our results help to understand the underlying failure mechanisms of the batteries caused by extreme heat and can help the design of the newer, safer generation of LIB cells.

Conflict of Interest

The authors declare no conflict of interest.

Data Availability Statement

The data that support the findings of this study are available on request from the corresponding author. The data are not publicly available due to privacy or ethical restrictions.

[1] F. Larsson, B.-E. Mellander, *J. Electrochem. Soc.* **2014**, *161*, A1611.

[2] C. F. Lopez, J. A. Jeevarajan, P. P. Mukherjee, *J. Electrochem. Soc.* **2015**, *162*, A2163.

[3] D. Di Lecce, S. Levchenko, F. Iacoviello, D. J. L. Brett, P. R. Shearing, J. Hassoun, *ChemSusChem* **2019**, *12*, 3550.

[4] H. Villarraga-Gómez, D. L. Begun, P. Bhattad, K. Mo, M. Norouzi Rad, R. T. White, S. T. Kelly, *Nondestr. Test. Eval.* **2022**, *37*, 519.

[5] R. F. Ziesche, T. Arlt, D. P. Finegan, T. M. M. Heenan, A. Tengattini, D. Baum, N. Kardjilov, H. Markötter, I. Manke, W. Kockelmann, D. J. L. Brett, P. R. Shearing, *Nat. Commun.* **2020**, *11*, 777.

[6] L. Vásárhelyi, Z. Kónya, Á. Kukovecz, R. Vajtai, *Mater. Today Adv.* **2020**, *8*, 100084.

[7] J. Zhu, X. Zhang, E. Sahraei, T. Wierzbicki, *J. Power Sources* **2016**, *336*, 332.

[8] T. Yokoshima, D. Mukoyama, F. Maeda, T. Osaka, K. Takazawa, S. Egusa, S. Naoi, S. Ishikura, K. Yamamoto, *J. Power Sources* **2018**, *393*, 67.

[9] D. P. Finegan, M. Scheel, J. B. Robinson, B. Tjaden, I. Hunt, T. J. Mason, J. Millichamp, M. Di Michiel, G. J. Offer, G. Hinds, D. J. L. Brett, P. R. Shearing, *Nat. Commun.* **2015**, *6*, 6924.

[10] D. P. Finegan, M. Scheel, J. B. Robinson, B. Tjaden, M. Di Michiel, G. Hinds, D. J. L. Brett, P. R. Shearing, *Phys. Chem. Chem. Phys.* **2016**, *18*, 30912.

[11] L. Salvo, M. Suéry, A. Marmottant, N. Limodin, D. Bernard, *C. R. Phys.* **2010**, *11*, 641.

[12] D. P. Finegan, E. Tudisco, M. Scheel, J. B. Robinson, O. O. Taiwo, D. S. Eastwood, P. D. Lee, M. Di Michiel, B. Bay, S. A. Hall, G. Hinds, D. J. L. Brett, P. R. Shearing, *Adv. Sci.* **2016**, *3*, 1500332.

[13] T. M. M. Heenan, C. Tan, J. Hack, D. J. L. Brett, P. R. Shearing, *Mater. Today* **2019**, *31*, 69.

[14] D. S. Eastwood, R. S. Bradley, F. Tariq, S. J. Cooper, O. O. Taiwo, J. Gelb, A. Merkle, D. J. L. Brett, N. P. Brandon, P. J. Withers, P. D. Lee, P. R. Shearing, *Nucl. Instrum. Methods Phys. Res., Sect. B* **2014**, *324*, 118.

[15] P. Shearing, D. Eastwood, R. Bradley, J. Gelb, S. Cooper, F. Tariq, P. Lee, *Microsc. Anal.* **2013**, *27*, 19.

[16] C. Lim, B. Yan, L. Yin, L. Zhu, *Energies* **2014**, *7*, 2558.

[17] L. Kong, X. Hu, G. Gui, Y. Su, M. Pecht, *Fire Technol.* **2020**, *56*, 2565.

[18] R. Carter, B. Huhman, C. T. Love, I. V. Zenyuk, *J. Power Sources* **2018**, *381*, 46.

[19] A. Yermukhambetova, C. Tan, S. R. Daemi, Z. Bakenov, J. A. Darr, D. J. L. Brett, P. R. Shearing, *Sci. Rep.* **2016**, *6*, 35291.

[20] Batteries Europe ETIP, *Eur. Technol. Innovation Platform* **2020**, 9.

[21] World Economic Forum, *Global Battery Alliance, A Vision for a Sustainable Battery Value Chain in 2030*, Global Battery Alliance **2019**, pp. 10–11, www.weforum.org.

[22] M. A. Sőrés, B. Hartmann, *J. Energy Storage* **2022**, *56*, 105959.

[23] S. Chen, Z. Gao, T. Sun, *Energy Sci. Eng.* **2021**, *9*, 1647.

[24] M. T. M. Pham, J. J. Darst, W. Q. Walker, T. M. M. Heenan, D. Patel, F. Iacoviello, A. Rack, M. P. Olbinado, G. Hinds, D. J. L. Brett, E. Darcy, D. P. Finegan, P. R. Shearing, *Cell Rep. Phys. Sci.* **2021**, *2*, 100360.

[25] P. Blazek, P. Westenberger, S. Erker, A. Brinek, T. Zikmund, D. Rettenwander, N. P. Wagner, J. Keckes, J. Kaiser, T. Kazda, P. Vyroubal, M. Macak, J. Todt, *J. Energy Storage* **2022**, *52*, 104563.

[26] Z. Lu, X. L. Yu, L. C. Wei, F. Cao, L. Y. Zhang, X. Z. Meng, L. W. Jin, *Appl. Therm. Eng.* **2019**, *158*, 113800.

[27] N. Meddings, M. Heinrich, F. Overney, J. S. Lee, V. Ruiz, E. Napolitano, S. Seitz, G. Hinds, R. Raccichini, M. Gaberšček, J. Park, *J. Power Sources* **2020**, *480*, 228742.

[28] M. Gaberšček, *Nat. Commun.* **2021**, *12*, 19.

[29] Y. Li, B. Dong, T. Zerrin, E. Jauregui, X. Wang, X. Hua, D. Ravichandran, R. Shang, J. Xie, M. Ozkan, C. S. Ozkan, *Energy Storage* **2020**, *2*, e186.

[30] T. Stockley, K. Thanapalan, M. Bowkett, J. Williams, M. Hathway, *IFAC Proc.* **2014**, *47*, 8610.

[31] J. G. Zhu, Z. C. Sun, X. Z. Wei, H. F. Dai, *RSC Adv.* **2014**, *4*, 29988.

[32] Q. Yang, J. Xu, B. Cao, X. Li, *PLoS One* **2017**, *12*, 0172424.

[33] L. A. Middlemiss, A. J. R. Rennie, R. Sayers, A. R. West, *Energy Rep.* **2020**, *6*, 232.

[34] W. Choi, H. C. Shin, J. M. Kim, J. Y. Choi, W. S. Yoon, *J. Electrochem. Sci. Technol.* **2020**, *11*, 1.

[35] E. P. Roth, D. H. Doughty, *J. Power Sources* **2004**, *128*, 308.

[36] D. Patel, J. B. Robinson, S. Ball, D. J. L. Brett, P. R. Shearing, *J. Electrochem. Soc.* **2020**, *167*, 090511.

[37] R. Li, J. Wu, H. Wang, G. Li, in *Proc. 2010 5th IEEE Conf. Industrial Electronics and Applications ICIEA 2010*, IEEE, Piscataway, NJ **2010**, pp. 684–688.

2300207 (10 of 10)